Hindawi
Shock and Vibration
Volume 2018, Article ID 7469894, 10 pages
https://doi.org/10.1155/2018/7469894

Research Article

Dynamic Analysis of Vehicle Track Coupling Based on Double Beam Track Model

Yayun Qi, Huanyun Dai, Jianjin Yang, and Kun Xu

State Key Laboratory of Traction Power, Southwest Jiaotong University, Chengdu 0086 610031, China

Correspondence should be addressed to Yayun Qi; yayun_qi@163.com

Received 7 December 2017; Accepted 11 March 2018; Published 17 April 2018

Academic Editor: Evgeny Petrov

The rail was considered as double Timoshenko beam in this paper, applied to the vehicle track coupling dynamics model; the Hertz nonlinear method is used to calculate the wheel rail contact force. Wheel rail vertical force and response of vehicle are calculated by using the model under random irregularity and single harmonic excitation; at the same time, wheel rail force and vertical acceleration response of 3-order, 10-order, and 19-order wheel polygon were calculated. The results show that, under the excitation of random irregularity, the wheel rail vertical force of two models was very close in the low frequency band, and the response of the double beam model in the high frequency band of 200–1000 Hz is larger than the single beam model, and the acceleration and displacement responses of the double beam model are relatively close. Under a single harmonic excitation, the double beam model has a shorter wheel rail force attenuation time than that of the single beam model. And wheel rail force peak value of double beam model is 9% larger than that of single beam model. Similarly, the vertical displacement of the double beam model increased by 2.6%. Under the 3-order and 10-order wheel polygon excitation, vertical wheel rail peak force of double beam is, respectively, 37.5% and 50% larger than single beam model; the vertical frame acceleration amplitude is 1 g and 1.7 g; under the 19-order polygon wheel excitation, the difference of the wheel rail force between two models is very small, and the amplitude of acceleration of bogie is 2.3 g. And double beam model has more advantage in analyzing high frequency problems such as wheel polygonization.

1. Introduction

Train vehicle system and track system are interaction and coupling systems [1]. A lot of researches have been done on the dynamics of vehicle track coupling system. Zhai et al. used a three-dimensional vehicle track coupled dynamics model that is developed in which a typical railway passenger vehicle is modelled as a 35-degree-of-freedom multibody system. And the rail considered as Timoshenko beam [2]. Martínez-Casas et al. use a 3D track model based on the Moving Element Method (MEM) which is developed to replace the Timoshenko beam considered in earlier studies, adopting cyclic boundary conditions and Eulerian coordinates. Therefore, the MEM permits fixing the contact area in the middle of a finitely long track and refining the mesh only around the contact area, where the forces and displacements will be more significant [3]. Thompson and Jones use Euler beam and Timoshenko beam analysis of the vibration characteristic of vehicle track system in frequency domain [4]. Ling et al. established the model of the track which is a flexible one consisting of rails, sleepers, and ballasts. In the track model, rails are assumed to be Timoshenko beams supported by discrete sleepers, and the effects of vertical and lateral motions and rail roll on wheel/rail creepage are taken into account, but this did not explore the high frequency problems [5]. Baeza et al. developed track model based on a substructuring approach, where a modal description of each isolated rail and sleeper is adopted. The rail is considered as a Rayleigh-Timoshenko beam. And it is used to simulate vibration caused by wheel flat [6].

Some scholars have studied the high frequency vibration characteristics of vehicle track system, mainly through the finite element or single layer Timoshenko beam model to calculate the corresponding vehicle response and wheel rail force response. Zhang and Wei established the vehicle track model considering the rail as Timoshenko beam; through

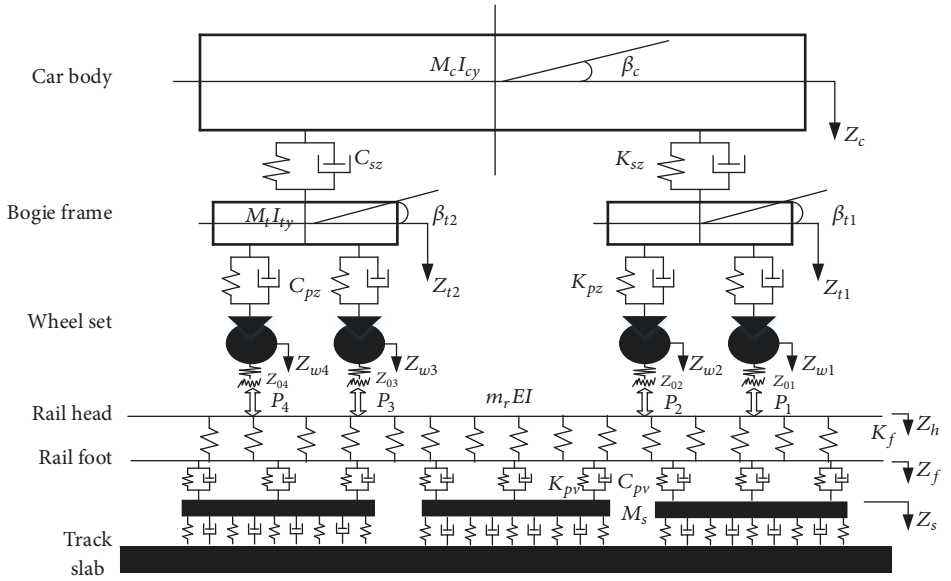

Figure 1: Dynamic model of vehicle track coupling system.

comparative analysis with Euler beam model, Timoshenko beam model is superior to the Euler model in case of exploring high frequency vibration of vehicle track system [7]. Wu et al. consider the track model is formulated with two rails supported on the discrete supports through the finite element method and analysis of the sleeper-passing-induced flexible vibration of wheel set [8]. Liu et al. established a coupling vibration model of vehicle track-subgrade system and established a 3D wheel system, as well as analysis of the vibration characteristic of wheel [9].

These methods consider rail as Euler beam or Timoshenko beam; through the establishment of vehicle track coupling dynamics equation, numerical integration method is used to get the vehicle dynamic response. Considering the track as a double layer Timoshenko beam model, the dynamic model of the double Timoshenko beam is established based on the vehicle track coupling dynamic model theory, and the dynamic response of the vehicle is calculated. The response of the double beam model is closer to that of the finite element model than the single beam model in the high frequency region. For the double beam model, we will consider the track as double Timoshenko beam and response of track system expression of the calculation, and finite element models are compared to verify that its accuracy is higher than single beam model in high frequency [10].

However, due to the emergence of some high frequency excitations such as wheel polygon, the characteristics of the double Timoshenko beam model need further exploration.

2. Model Establishment

2.1. Vehicle Model. In the vehicle model, ten degrees of freedom are considered in total, including the car body's nodding and bouncing, the bogie frame's nodding and bouncing movement, and the wheelset's bouncing. The rail is considered as double Timoshenko beam model of vehicle track coupling dynamics diagram as shown in Figure 1.

Car Body Pitch Motion

$$M_c\ddot{Z}_c + 2C_{sz}\dot{Z}_c + 2K_{sz}Z_c - C_{sz}\dot{Z}_{t1} - K_{sz}Z_{t1} - C_{sz}\dot{Z}_{t2} - K_{sz}Z_{t2} - M_cg = 0. \quad (1)$$

Car Body Bounce Motion

$$J_c\ddot{\beta}_c + 2C_{sz}l_c^2\dot{\beta}_c + 2K_{sz}l_c^2\beta_c - C_{sz}l_c\dot{Z}_{t1} - K_{sz}l_cZ_{t1} - C_{sz}l_c\dot{Z}_{t2} - K_{sz}l_cZ_{t2} = 0. \quad (2)$$

The equation of motions for the front ($i = 1$) and rear ($i = 2$) bogie frame in the vertical and pitch directions can be expressed as follows.

Front Bogie Pitch Motion

$$M_t\ddot{Z}_{t1} + \left(2C_{pz} + C_{sz}\right)\dot{Z}_{t1} + \left(2K_{pz} + K_{sz}\right)Z_{t1} - C_{sz}\dot{Z}_c - K_{sz}Z_c - C_{pz}\dot{Z}_{w1} - C_{pz}\dot{Z}_{w2} - K_{pz}Z_{w1} - K_{pz}Z_{w2} + C_{sz}l_c\dot{\beta}_c + K_{sz}l_c\beta_c - M_tg = 0. \quad (3)$$

Front Bogie Bounce Motion

$$J_t\ddot{\beta}_{t1} + 2C_{pz}l_t^2\dot{\beta}_{t1} + 2K_{pz}l_t^2\beta_{t1} + C_{pz}l_t\dot{Z}_{w1} - C_{pz}l_t\dot{Z}_{w2} + K_{pz}l_tZ_{w1} - K_{pz}l_tZ_{w2} = 0. \quad (4)$$

Rear Bogie Pitch Motion

$$M_t\ddot{Z}_{t2} + \left(2C_{pz} + C_{sz}\right)\dot{Z}_{t2} + \left(2K_{pz} + K_{sz}\right)Z_{t2} - C_{sz}\dot{Z}_c - K_{sz}Z_c - C_{pz}\dot{Z}_{w3} - C_{pz}\dot{Z}_{w4} - K_{pz}Z_{w3} - K_{pz}Z_{w4} + C_{sz}l_c\dot{\beta}_c + K_{sz}l_c\beta_c - M_tg = 0. \quad (5)$$

Rear Bogie Bounce Motion

$$J_t\ddot{\beta}_{t2} + 2C_{pz}l_t^2\dot{\beta}_{t2} + 2K_{pz}l_t^2\beta_{t2} + C_{pz}l_t\dot{Z}_{w3} - C_{pz}l_t\dot{Z}_{w4} + K_{pz}l_tZ_{w3} - K_{pz}l_tZ_{w4} = 0. \quad (6)$$

First Wheelset Pitch Motion

$$M_w\ddot{Z}_{w1} + C_{pz}\dot{Z}_{w1} + K_{pz}Z_{w1} - C_{pz}\dot{Z}_{t1} - K_{pz}Z_{t1} + C_{pz}l_t\ddot{\beta}_{t1} + K_{pz}l_t\beta_{t1} - M_wg - P_{w1} = 0. \quad (7)$$

Second Wheelset Pitch Motion

$$M_w\ddot{Z}_{w2} + C_{pz}\dot{Z}_{w2} + K_{pz}Z_{w2} - C_{pz}\dot{Z}_{t1} - K_{pz}Z_{t1} - C_{pz}l_t\ddot{\beta}_{t1} - K_{pz}l_t\beta_{t1} - M_wg - P_{w2} = 0. \quad (8)$$

Third Wheelset Pitch Motion

$$M_w\ddot{Z}_{w3} + C_{pz}\dot{Z}_{w3} + K_{pz}Z_{w3} - C_{pz}\dot{Z}_{t2} - K_{pz}Z_{t2} + C_{pz}l_t\ddot{\beta}_{t2} + K_{pz}l_t\beta_{t2} - M_wg - P_{w3} = 0. \quad (9)$$

Fourth Wheelset Pitch Motion

$$M_w\ddot{Z}_{w4} + C_{pz}\dot{Z}_{w4} + K_{pz}Z_{w4} - C_{pz}\dot{Z}_{t2} - K_{pz}Z_{t2} - C_{pz}l_t\ddot{\beta}_{t2} - K_{pz}l_t\beta_{t2} - M_wg - P_{w4} = 0. \quad (10)$$

2.2. Rail Model. According to the Timoshenko beam theory, the partial differential equations of the bending vibration and cross section rotation of the rail under wheel rail force can be expressed as follows [1].

Vertical Vibration

$$\begin{aligned} &m\frac{\partial^2 z(x,t)}{\partial t^2} + \kappa_z GA\left[\frac{\partial \psi_z(x,t)}{\partial x} - \frac{\partial^2 z(x,t)}{\partial x^2}\right] = -\sum_{i=1}^{N_s} F_{szi}\delta(x_{si}) \\ &+ \sum_{j=1}^{N_w} F_{wrzj}\delta\left(x_{wj}\right), \\ &\rho I_y\frac{\partial^2 \psi_z(x,t)}{\partial t^2} + \kappa_z GA\left[\psi_z(x,t) - \frac{\partial z(x,t)}{\partial x}\right] \\ &- EI_y\frac{\partial^2 \psi_z(x,t)}{\partial x^2} = 0, \end{aligned} \quad (11)$$

where z is the rail vertical displacement; ψ_z is rail section rotation angel around z-axis; F_{szi} is the support force; F_{wrzj} is the wheel rail vertical load; I_y is the moment of inertia of rail section of y-axis; I_z is the second moment of rail cross section of z-axis; ρ is density per unit length of the rail; G is rail to rail section shear modulus; A is rail cross area; κ_z is vertical shear coefficient.

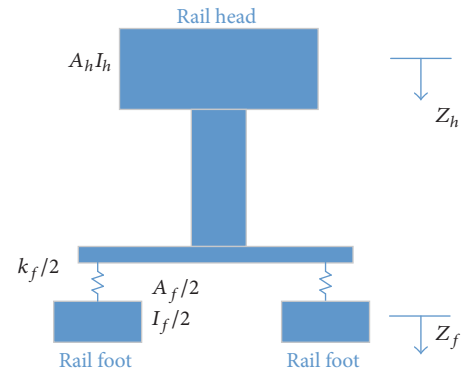

Figure 2: Sketch map of track double beam model.

By using the method of separation of variables, the vertical displacement of rail can be expressed as regular mode shape function and regular coordinate:

$$\begin{aligned} z(x,t) &= \sum_{k=1}^{NMZ} Z_k(x)\, q_{zk}(t), \\ \psi_z(x,t) &= \sum_{k=1}^{NMZ} \Psi_{zk}(x)\, w_{zk}(t). \end{aligned} \quad (12)$$

The traditional track model will be considered as single Timoshenko beam or Euler beam; in this paper we will consider the track as double Timoshenko beam, which is divided into two parts of the rail head and rail base. Continuous elastic connection between rail top and rail base. The schematic diagram of the track double beam model is shown in Figure 2. This model can better reflect the high frequency response of the track.

Based on the orthogonality of the regular mode shapes and the Dirac function, the ordinary differential equations of the double beam model on regular coordinates can be obtained.

Vertical Vibration of Rail Top Beam (Rail Top)

$$\begin{aligned} &\ddot{q}_{zkh}(t) + \frac{\kappa_h GA_h}{m}\left(\frac{k\pi}{l}\right)^2 q_{zkh}(t) - \kappa_h GA_h\frac{k\pi}{l} \cdot \sqrt{\frac{1}{m\rho I_h}}\omega_{zkh}(t) = -\sum_{i=1}^{N_s} F_{fzi}Z_k(x_{si}) \\ &+ \sum_{j=1}^{N_w} F_{wrzj}Z_k\left(x_{wj}\right), \\ &\ddot{\omega}_{zkh}(t) + \left[\frac{\kappa_z GA_h}{\rho I_y} + \frac{E}{\rho}\left(\frac{k\pi}{l}\right)^2\right]\omega_{zkh}(t) \\ &- \kappa_h GA_h\frac{k\pi}{l}\sqrt{\frac{1}{m\rho I_h}}q_{zkh}(t) = 0. \end{aligned} \quad (13)$$

Table 1: Vehicle parameters.

Notation	Specification	Value
M_c	Car body mass (kg)	33766
M_t	Bogie mass (kg)	2200
M_w	Wheelset mass (kg)	1550
J_c	Mass moment of inertia of car body (kg m^2)	$1655.5 * 10^3$
J_t	Mass moment of inertia of bogie frame (kg m^2)	2590
K_{pz}	Stiffness of primary suspension (N/m)	886.5 KN/m
K_{sz}	Stiffness of secondary suspension (N/m)	203 KN/m
C_{pz}	Damping coefficient of primary suspension (N s/m)	10 KN·s/m
C_{sz}	Damping coefficient of secondary suspension (N s/m)	58 KN·s/m
l_c	Semilongitudinal distance between bogies (m)	8.75 m
l_t	Semilongitudinal distance between wheelsets in bogie (m)	1.25 m

Table 2: Rail parameters.

Notation	Specification	Value
E	Elastic modulus of rail (MPa)	2.059×10^5
ρ	Density	7850
A_h	The area of rail head	$7.09e-3$
I_h	The second moment of area of the rail head section about the z-axis	$30.4e-6$
A_f	Area of rail base	$0.6e-3$
I_f	The second moment of area of the rail base section about the z-axis.	$0.118e-6$
ls	Sleeper spacing (m)	0.6
κ_h	Vertical shear coefficient of rail head	0.45
κ_f	Vertical shear coefficient of rail base	0.85

Vertical Vibration of Rail Bottom Beam (Rail Base)

$$\ddot{q}_{zkf}(t) + \frac{\kappa_f G A_f}{m}\left(\frac{k\pi}{l}\right)^2 q_{zkf}(t) - \kappa_z G A_f \frac{k\pi}{l} \cdot \sqrt{\frac{1}{m\rho I_f}}\omega_{zkf}(t) = \sum_{i=1}^{N_s} F_{fzi} Z_k(x_{si}) - \sum_{i=1}^{N_s} F_{szi} Z_k(x_{si}), \tag{14}$$

$$\ddot{\omega}_{zkf}(t) + \left[\frac{\kappa_f G A_f}{\rho I_f} + \frac{E}{\rho}\left(\frac{k\pi}{l}\right)^2\right]\omega_{zkf}(t) - \kappa_f G A_f \frac{k\pi}{l}\sqrt{\frac{1}{m\rho I_f}} q_{zkf}(t) = 0.$$

Here A_h is the area of rail head; I_h is the second moment of area of the rail head section about the z-axis. A_f is the area of rail base; I_f is the second moment of area of the rail base section about the z-axis. F_{fzi} is supporting force between rail top and rail bottom. κ_h is vertical shear coefficient of rail head. κ_f is vertical shear coefficient of rail base:

$$F_{fzi} = k_f\left(Z_h - Z_f\right). \tag{15}$$

Here, Z_h is the vertical displacement of rail head; Z_f is the vertical displacement of rail base.

The regular mode shape function of the Timoshenko beam with two ends simply supported is

$$Z_k = \sqrt{\frac{2}{ml}}\sin\left(\frac{k\pi}{l}x\right), \quad \Psi_{zk}(x) = \sqrt{\frac{2}{\rho I_y l}}\cos\left(\frac{k\pi}{l}x\right). \tag{16}$$

The vehicle and rail parameters used in the simulation are shown in Tables 1 and 2.

2.3. Vertical Interaction between Wheel and Rail. The normal force of the wheel and rail is solved by Hertz nonlinear elastic contact theory, and the expression is as follows:

$$F_N(t) = \begin{cases} \left[\frac{1}{G}\delta Z(t)\right]^{3/2}, & \delta Z(t) > 0 \\ 0, & \delta Z(t) \le 0. \end{cases} \tag{17}$$

G is the wheel rail contact constant (m/N$^{2/3}$), the wear wheel (CN60) can be used to calculate $G = 3.86R^{-0.115} \times 10^{-8}$, and $\delta Z(t)$ is the penetration of wheel rail contact point.

2.4. Zhai Method. The vehicle system model and the track system model can be represented by the following expressions:

$$M\ddot{X}(t) + C\dot{X}(t) + KX(t) = F(t). \tag{18}$$

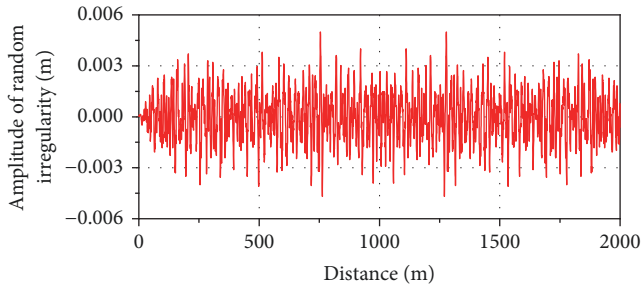

Figure 3: Measured track irregularity (vertical).

In the formula, M, C, and K represent the mass, stiffness, and damping matrices, respectively, $\ddot{X}(t)$ $\dot{X}(t)$ $X(t)$ represent acceleration, velocity, and displacement vectors. $F(t)$ represent force vector. In order to solve such large-scale system model, Zhai method is adopted [1]:

$$X_{n+1} = X_n + \dot{X}_n \Delta t + \left(\frac{1}{2} + \alpha\right) \ddot{X}_n \Delta t^2 - \alpha \ddot{X}_{n-1} \Delta t^2,$$
$$\dot{X}_{n+1} = \dot{X}_n + \left(\frac{1}{2} + \beta\right) \ddot{X}_n \Delta t - \beta \ddot{X}_{n-1} \Delta t. \tag{19}$$

In order to ensure the integral speed and accuracy, α and β are the integral control parameters, usually 0.5, and Δt is the integral step length: $n, n-1, n+1$. They represent the current step $n\Delta t$, the last step $(n-1)\Delta t$, and the next integral moment $(n+1)\Delta t$.

3. Comparative Analysis

In order to compare the dynamic response under random track irregularity, a high speed line measured track irregularity (Figure 3) and a single harmonic irregularity were chosen as input excitations, through the model established in Section 2, using the same parameters, compared to vehicle's vertical vibration response between double Timoshenko beam model and single Timoshenko beam model; the results are as shown in Figures 4–6. Wheel rail vertical force, vertical acceleration of wheelset, and vertical displacement of rail are calculated in time-domain and frequency domain.

From Figures 4–6 it can be seen that the response of wheel rail vertical force, vertical acceleration of wheelset, and vertical displacement of rail in the time-domain has little difference. While the response of wheel rail vertical force in the frequency domain has obvious difference, the single beam model and double beam model results have little difference in the frequency band of 0–200 Hz, while larger difference in the high frequency band of 200–1000 Hz especially in the vicinity of a rail pined-pined frequency double beam model has significantly large vibration response, the first-order "pined-pined" frequency of rail has great effects on the vibration and noise radiation [11]. This is because the rail single layer beam model cannot consider the cross section deformation of rail. When considering the rail as a double layer beam model, the relative motion between rail top and rail bottom can be considered. The high frequency vibration response of rail is influenced by rail cross section deformation [12]. Therefore, the double layer beam model can better reflect the high frequency vibration response of rail. In high frequency zone, double beam model considers cross section deformation of rail and has a more realistic result. The response of random track irregularity can show the inherent property of the track. When considering the high frequency problems, double beam model has more advantage.

The response of single harmonic excitation is shown in Figures 7 and 8. The single harmonic wavelength is 0.1 m, and the wave depth is 0.2 mm. The response from a single harmonic wheel rail force and wheel vertical displacement can be seen under the same harmonic excitation; the vertical wheel/rail force of double beam model attenuation is faster than single beam model; wheel rail vertical force peak of double beam model is 9% bigger than single beam model; this is because the rail double beam model considers the relative movement between the rail bottom and the rail top, and rail stiffness decreases, which decays faster, and the vertical wheel/rail force amplitude is larger. The vertical displacement peak value of the double beam model wheel is 2.6% larger than that of the single layer beam, because the double layer beam model takes into account the section deformation of rail, and then the rail stiffness decreases, and the vertical displacement of wheelset increases.

4. Model Response under Polygonal Excitation

4.1. Wheel Polygon Model. There are many methods for wheel polygon simulation; one of the most common methods is to expand the radial deviation of the wheel into a Fourier series form and then equivalently stack it into the track irregularities and wheelset remains unchanged. Another method is to change the circumference of the wheel, and the harmonic function is used to simulate the change of circumference; the equations are as follows:

$$\Delta r = A \sin\left(n\beta + \beta_0\right),$$
$$r\left(\beta\right) = R - \Delta r, \tag{20}$$
$$\beta\left(t\right) = \beta\left(t-1\right) + \omega \Delta t,$$

where A is the magnitude of the noncircularity, n is the polygon number of wheels, which means the number of harmonic cycles formed by the difference between the actual radius and the nominal radius of the wheel within 360 degrees of the wheel. β is wheel corner, β_0 is the phase angle, r is the wheel diameter difference along the wheel circumference, and R is the nominal rolling radius of the wheel. By modifying the orders and magnitude of wheel polygons, different wheel polygon conditions can be simulated.

4.2. Measurement of Wheel Polygon Irregularity. The wheel polygon wear brings many problems to the high speed train operation. The current research mainly focuses on the two aspects of polygon's influence on dynamics and polygon wear mechanism. Johansson and Andersson established a three-dimensional wheel rail interaction model and used it to simulate the wear of out-of-roundness problem [13]. Morys

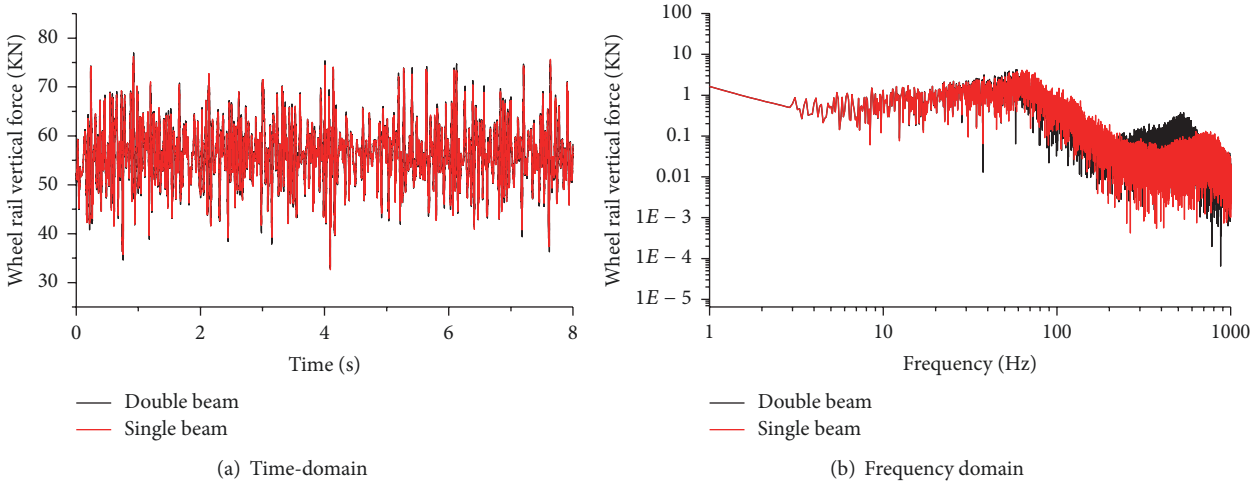

Figure 4: Comparison of wheel rail force.

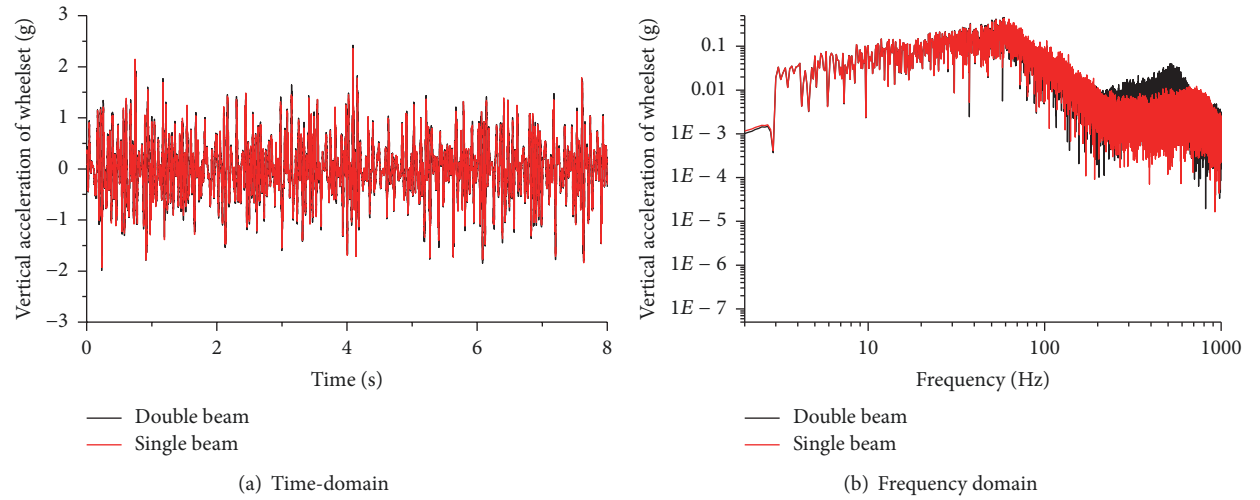

Figure 5: Vertical acceleration of wheelset.

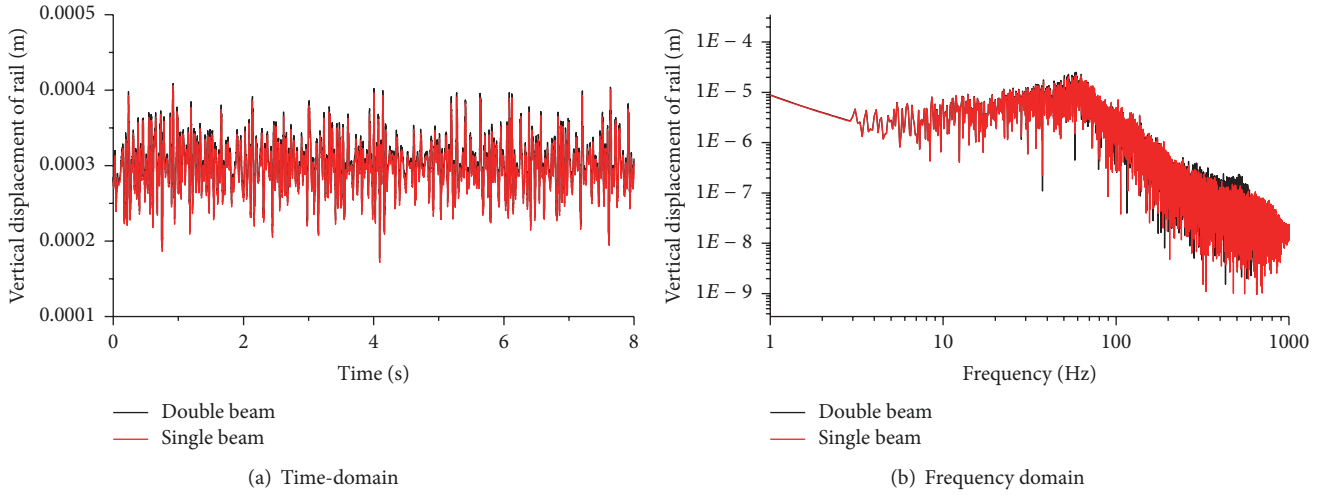

Figure 6: Vertical displacement of rail.

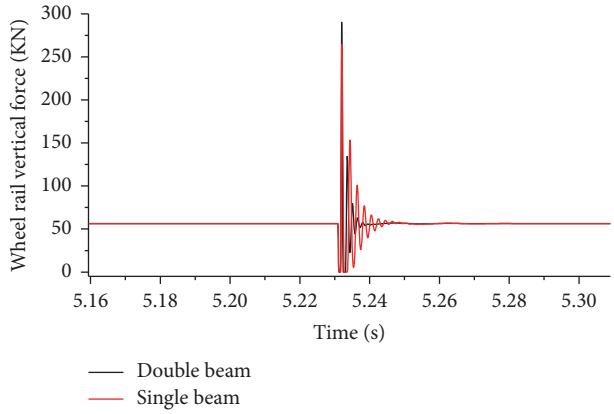

Figure 7: Wheel rail force response under single harmonic.

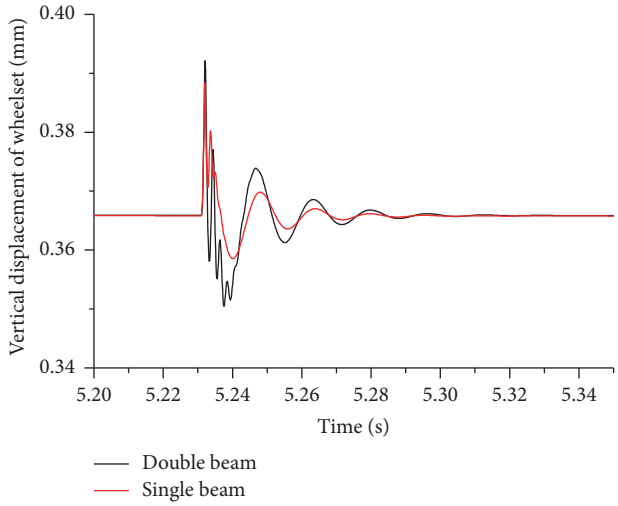

Figure 8: Wheelset vertical displacement under single harmonic response.

established a vehicle track model to analyze the origin and the enlargement of OOR phenomena [14]. P. Meinke and S. Meinke formulated a dynamic model to study the influences of the static and dynamic imbalances on the polygonalisation of wheel treads [15]. In the vehicle track coupling dynamics system, the polygon excitation of the wheel is transformed into the vertical excitation between the wheel and rail when the polygonal wear is simulated. And then vehicle track system model is used to calculate the response of the two models. The following is the polygon wear of the 1 wheel wheelset and the right wheel measured by a certain type of high speed EMU in China. The wheel polygon amplitude and the roughness levels of different orders are given, as shown in Figure 9. It can be seen from the figure that the wheel wear is mainly caused by 19-order wear. It was the most commonly out-of-roundness wheel wear order in China's high speed way. So it was chosen as a simulation object.

The wheel rail vertical force and the acceleration response of the wheel and rail under the polygon excitations of the 3, 10, and 19 orders are calculated, respectively, as shown in Figures 10–12. Through the calculation we can see that, in the 3-order polygon under the effect of the frequency which is 92.7 Hz, wheel rail force amplitude of single beam and double beam is different; double beam wheel rail force amplitude increases by 37.5%. Frame acceleration amplitude is within 1 g, with double beam and single beam difference. In the 10-order polygon under the action of 308 Hz main frequency, wheel rail vertical force amplitude of double beam model is 50% larger than single beam; in the 2 octave 616 Hz double beams wheel rail force amplitude is far greater than the single beam model, frame acceleration amplitude is 1.7 g, and double beam model is slightly larger than the single beam. Under the excitation of 19-order polygon, the vertical force amplitude of the double beam model is different from that of the single beam under the dominant frequency of 586 Hz. The acceleration amplitude of the frame is 2.3 g, and the vertical acceleration of the two model frames has little difference.

5. Conclusions

In this paper, a double Timoshenko beam model is established, and the wheel rail force and vehicle dynamic response

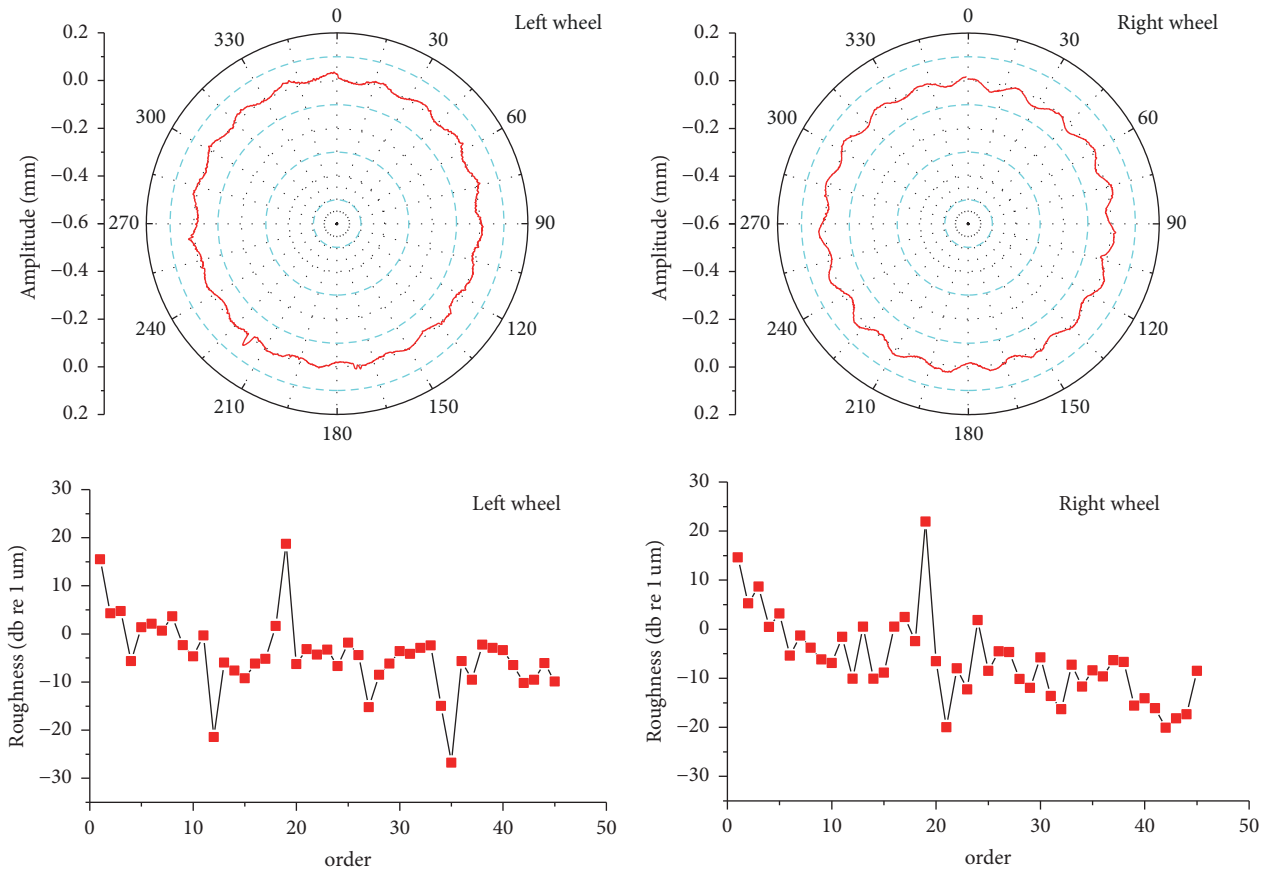

FIGURE 9: Polygon of measured wheel.

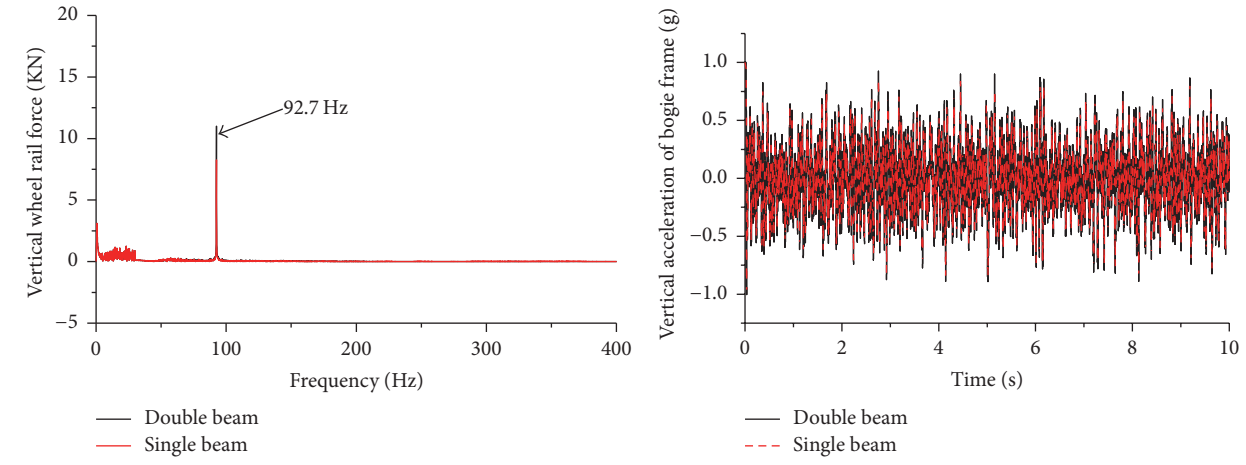

(a) Wheel rail vertical force

(b) Vertical acceleration of the framework

FIGURE 10: Wheel/rail force and frame acceleration response of 3-order wheel polygon.

under different excitations are calculated by numerical integration method.

(1) Under the random irregularity excitation, when the rail is considered as a double beam model, the relative motion between the rail top and the bottom of the rail was considered. At the band of 0–200 Hz, the results of single beam model and double beam model are similar, but with great differences in the high frequency section of 200 Hz–1000 Hz, especially in the vicinity of the first-order "pined-pined" frequency of rail. So the double beam model can reflect the high frequency characteristics of rail.

(2) Under the short wave harmonic excitation, the double beam model considering deformation of rail, the vertical stiffness decreases, so the decay time of the double beam

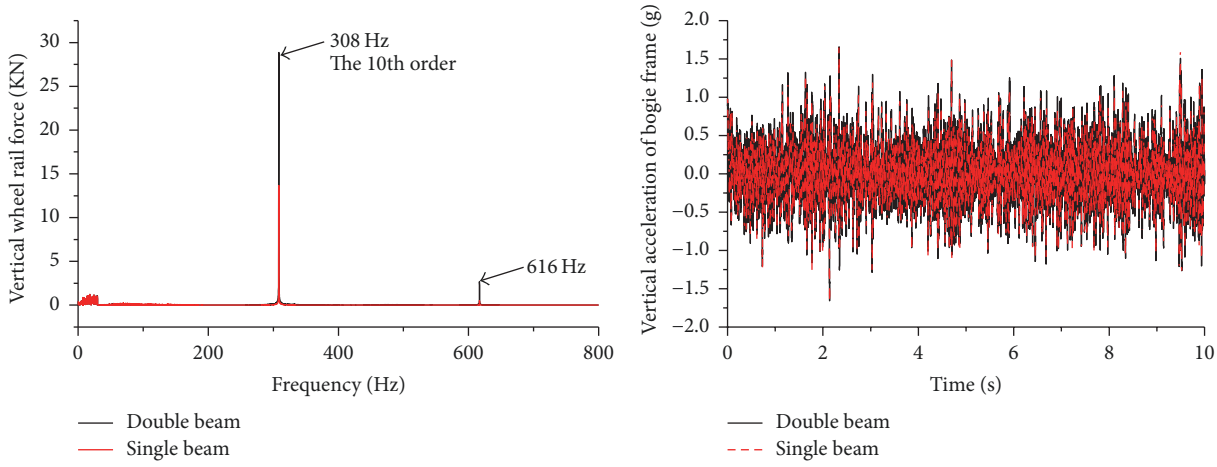

(a) Wheel rail vertical force (b) Vertical acceleration of the framework

Figure 11: Wheel/rail force and frame acceleration response of 10-order wheel polygon.

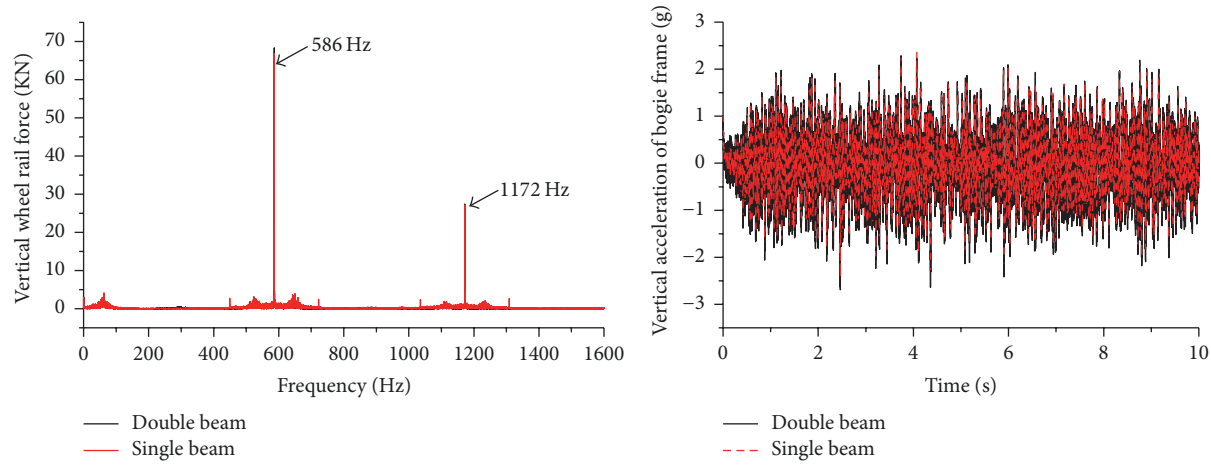

(a) Wheel rail vertical force (b) Vertical acceleration of the framework

Figure 12: Wheel/rail force and frame acceleration response of 19-order wheel polygon.

model is shorter than the single beam model; the wheel rail vertical force peak value of double beam model is 9% bigger than single beam model; the wheelset vertical displacement peak value of double beam model is 2.6% larger than single beam model.

(3) Under the polygon wheel excitation, we can see under the 3-order polygon wheel excitation that the wheel rail vertical force peak value of double beam model is 37.7% bigger than the single beam model; the vertical acceleration amplitude is 1 g. Under the 10-order wheel polygon the double beam model of wheel rail vertical force peak value is 50% bigger than the single beam model; the vertical acceleration amplitude is 1.7 g. Under the excitation of the 20-order wheel polygon, the amplitude of the vertical force of the wheel and rail of the double beam is close to the single beam, and the vertical acceleration of the frame is 2.3 g. The vertical acceleration amplitude of the double beam model is slightly larger than that of the single beam model under the three different wheel polygon orders.

Through analysis of the vibration characteristics of the random irregularity excitation, short wave harmonic excitation, and polygon wheel excitation, we can see that when considering the vertical deformation between rail head and rail foot, it is easier to cause the high frequency vibration of the rail, and double beam model is more accurate than single beam model in analysis of high frequency problems such as wheel polygonization.

Conflicts of Interest

The authors declare that there are no conflicts of interest regarding the publication of this paper.

Acknowledgments

The authors gratefully acknowledge the support from the China Railway General Corporation Foundation under Grants no. 2016J001-B and no. 2016G008-A.

References

[1] W. Zhai, *Vehicle-track coupled dynamics*, vol. 1, Science Press, Beijing, China, 4th edition, 2015.

[2] W. Zhai, K. Wang, and C. Cai, "Fundamentals of vehicle-track coupled dynamics," *Vehicle System Dynamics*, vol. 47, no. 11, pp. 1349–1376, 2009.

[3] J. Martínez-Casas, J. Giner-Navarro, L. Baeza, and F. D. Denia, "Improved railway wheelset-track interaction model in the high-frequency domain," *Journal of Computational and Applied Mathematics*, vol. 309, pp. 642–653, 2017.

[4] D. Thompson and C. Jones, "Reply to comments on chapter 12 of "railway noise and vibration: Mechanisms, modelling and means of control", by D. thompson (with contributions from C. jones and P.-E. gautier), elsevier, 2009," *Applied Acoustics*, vol. 72, no. 10, pp. 787-788, 2011.

[5] L. Ling, X. Xiao, J. Xiong, L. Zhou, and Z. Wen, "A 3D model for coupling dynamics analysis of high-speed train/track system," *Journal of Zhejiang University Science A*, vol. 15, no. 12, pp. 964–983, 2014.

[6] L. Baeza, A. Roda, and J. C. O. Nielsen, "Railway vehicle/track interaction analysis using a modal substructuring approach," *Journal of Sound and Vibration*, vol. 293, no. 1-2, pp. 112–124, 2006.

[7] Y. Zhang and W. Wei, "Study of Vertical Coupling Dynamics of Vehicle and Track Systems for high Frequency," *Journal of Dalian Railway Institute*, vol. 27, no. 2, pp. 9–12, 2006.

[8] X. Wu, W. Cai, M. Chi, L. Wei, H. Shi, and M. Zhu, "Investigation of the effects of sleeper-passing impacts on the high-speed train," *Vehicle System Dynamics*, vol. 53, no. 12, pp. 1902–1917, 2015.

[9] L. Liu, H. Liu, and X. Lei, "High frequency vibration characteristics of wheels in wheel-rail system," *Journal of Traffic and Transportation Engineering*, vol. 11, no. 6, pp. 44–49, 2011.

[10] T. X. Wu and D. J. Thompson, "A double Timoshenko beam model for vertical vibration analysis of railway track at high frequencies," *Journal of Sound and Vibration*, vol. 224, no. 2, pp. 329–348, 1999.

[11] D. J. Thompson, *Wheel-rail noise: theoretical modelling of the generation of vibrations [Ph.D. thesis]*, University of Southampton, Southampton, England, 1990.

[12] D. J. Thompson, "Wheel-rail noise generation, part III: rail vibration," *Journal of Sound and Vibration*, vol. 161, no. 3, pp. 421–446, 1993.

[13] A. Johansson and C. Andersson, "Out-of-round railway wheels—a study of wheel polygonalization through simulation of three-dimensional wheel-rail interaction and wear," *Vehicle System Dynamics*, vol. 43, no. 8, pp. 539–559, 2005.

[14] B. Morys, "Enlargement of out-of-round wheel profiles on high speed trains," *Journal of Sound and Vibration*, vol. 227, no. 5, pp. 965–978, 1999.

[15] P. Meinke and S. Meinke, "Polygonalization of wheel treads caused by static and dynamic imbalances," *Journal of Sound and Vibration*, vol. 227, no. 5, pp. 979–986, 1999.